理學碩士 學位論文

칼슘 양이온에 의한 캘릭스퀴논의
수용액에서의 전기화학 거동 변화

Electrochemistry of Calix[4]quinone Altered

by Ca^{2+} Ion in Water

2014 年 8 月

서울大學校 大學院

化學部 分析化學專攻

金 素 英

Abstract

Calix[4]arene-triacid-monoquinone (CTAQ), a quinone-containing water-soluble ionophore, was utilized to investigate how the proton-coupled electron transfer (PCET) reaction of quinone in water would be altered by a redox-inactive metal ion. This ionophoric quinone derivative captured a Ca^{2+} ion, which drastically changed the voltammetric behavior of the quinone. Its characteristic response to pH and unique redox potential separation allowed us to decipher the underlying mechanism. Spectroelectrochemistry verified significant stabilization of the semiquinone, and electrocatalytic currents were observed in the presence of Ca^{2+}-free CTAQ. Using digital simulation of cyclic voltammograms to clarify how the thermodynamic properties of quinones were altered, a simple scheme was proposed that successfully accounted for the observations. The change induced by Ca^{2+} complexation was explained on the basis of the combined effects of electrostatic influence of the captured metal ion and hydrogen bonding of water molecules with the support of DFT calculation.

This work was accomplished in collaboration with Prof. Suk-kyu Chang's group (Chung-Ang Univ.) and Prof. Jin Yong Lee's group (Sungkyunkwan Univ.). Synthesis of CTAQ and DFT calculation were contributed by Prof. Chang and Prof. Lee, respectively. Most part of this thesis is verbatim reproduction of an SCI paper by the author (*J. Am. Chem. Soc.,* **2013**, *135*, 18957).

Keywords : Quinone, Proton-coupled electron transfer (PCET), Metal ion-coupled electron transfer (MCET), Electrochemical investigation of mechanism, Digital simulation of cyclic voltammetry, Pourbaix diagram, Semiquinone radical

Student number : 2012-23037

Contents

1. Introduction

Quinone is a redox active organic moiety that plays diverse roles in many natural systems. It plays a key role in biological energy transduction via the electron transport chain in photosynthesis and respiration, is involved in the regulation of oxidative stress, performs antibiotic or anticancer activities, acts as signaling molecules, and many more. The reduction potentials and pK_a values of quinones, which determine their reactivity and stability, can be modulated to a large degree by different substituents, aromaticity or the surrounding chemical environment[1],[2]. In fact, nature delicately tunes these properties in order to drive the desired reactions and suppress unwanted reactions such as reactive oxygen species (ROS) generation[3],[4]. Consequently, an extensive body of research for over a hundred years has been devoted to the properties and reactions of quinones. Reduction potentials, pK_a values, rate constants and reaction mechanisms were probed. The influence of different substituents and aromaticity has been studied and good correlations with simple linear relationships have been established[5],[6]. The effect of solvents, hydrogen bonding and protonation have been studied in detail as well, in

nonaqueous, mixed, and aqueous solutions at different pHs and buffer concentrations[7]-[11].

Quinone reduction/oxidation is also a classic example of proton-coupled electron transfer (PCET). Electron transfer (ET) processes are often coupled to the transfer of protons to avoid unstable charge accumulation[12],[13]. Analogous to PCET, redox-inactive metal ions in the vicinity of redox centers can also influence ET, and the term metal ion-coupled electron transfer (MCET) was recently coined[14],[15]. Both protonation and metal ion binding bring about a positive shift in the reduction potential that depends on pK_a or binding constant difference. Redox-inactive metal ions such as Mg, Ca, Zn ions are important components in enzymes; in addition to providing structural support, they sometimes reside at active sites and take part in catalysis by activating the substrate electrophilically[16].

Electrochemistry of quinones is also sensitive to metal ion binding. Metal ions were found to stabilize the semiquinone radical anion $(Q^{\bullet-})$[17], enhancing intramolecular[18]-[20] and intermolecular[21],[22] one-electron transfers to quinone in aprotic solvents. There is a biological example that utilizes the

quinone-metal ion interaction; a series of dehydrogenases contain a Ca^{2+}-pyrroloquinoline quinone (PQQ) complex in the active sites[23]. The removal of Ca^{2+} ion resulted in loss of activity because electron transfer from the substrate to the quinone cofactor required the presence of a Ca^{2+} ion[24]. Searching for studies that probed metal ion influence on quinone PCET reactions in water, an electrochemical investigation of coenzyme Q (CoQ) derivatives was found to show that hydroxylated CoQ gives rise to Ca^{2+}-sensitive/pH-insensitive redox peak whereas the native CoQ shows Ca^{2+}-insensitive/pH-sensitive redox peak[25]. But in this example, proton and Ca^{2+} hardly compete with each other because hydroxyl and native CoQ have completely different properties in terms of pK_a and metal ion binding strength. Some studies observed that quinone autoxidation by oxygen was enhanced by metal ions[26]-[28]. But they were mostly limited to observation of apparent kinetics and provided no comprehensive picture about how metal ions affect the PCET reactions. Moreover, in existing studies the high dielectric constant of water or even polar organic solvents required addition of excess amount of metal ions so that complexities

arose from metal ion concentration dependency and different binding modes[19], and in nearly all cases quinones had to be ortho or hydroxylated to chelate metal ions.

For a straightforward assessment of metal ion influence on PCET in aqueous solutions, it would be desirable to anchor the metal ion near the redox center rather than let it ion-pair with it upon ET, eliminating the metal ion concentration dependence and simplifying the redox reaction. In this study, we utilized a quinone-containing water-soluble ionophore as a model compound, calix[4]arene-triacid-monoquinone (CTAQ, Fig. 1-1). Calixquinones were first synthesized in 1989[29] and expanded in diversity[30],[31] to a water-soluble version through the attachment of carboxylic acid groups to the lower rim[32]. These pendant carboxylates bind most metal ions effectively and little metal ion concentration dependency was found at >1 equiv of metal ions. Voltammetric behavior of CTAQ was also significantly altered by the presence of metal ions. Surprisingly, in weakly alkaline buffered solutions, binding of some metal ions such as Ca^{2+} caused the single two-electron redox wave of the quinone to split into two distinct waves that were attributed to separate one-electron transfer

steps[33]. Such a clear separation of electron transfer steps to quinone in buffered aqueous solutions is very rare; only a small separation was found in highly basic solutions where no protonation is involved[34],[35]. In spite of these interesting attributes of water-soluble calixquinone and its metal ion complexes, rigorous investigation of its PCET behavior was put off up to this day. This may be due to the fact that researchers were primarily concerned with analytical applications regarding calixquinones.

In the present study, a detailed account of the electrochemistry of CTAQ and Ca^{2+}-complexed CTAQ (CaCTAQ) in aqueous environment is given. Along with the biological significance of Ca^{2+}[36],[37], We chose to focus on Ca^{2+} after preliminary experiments with other metal ions, as will be explained below. Electrochemical methods were primarily employed as they are useful for thermodynamic investigation of PCET[38]. The nature of the unusual separation of faradaic reaction steps was verified with electrochemical and spectroscopic evidences. Digital simulation of voltammograms yielded quantitative estimates of the thermodynamic parameters involved, and simple arguments

based on those parameters led to the observation of electrocatalytic currents at less than 1 equiv of Ca^{2+}. The change induced by Ca^{2+} pointed to the crucial contribution of the surrounding aqueous environment, in addition to the effect of Ca^{2+} itself.
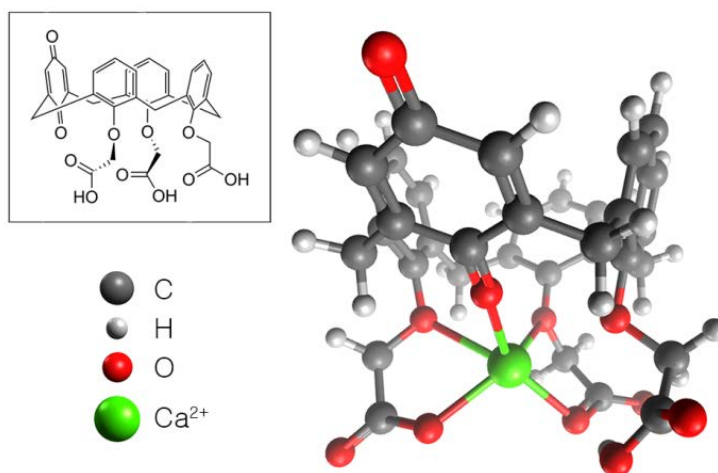

Fig. 1-1 The structures of (Inset, 2D) CTAQ and (3D) CaCTAQ. The geometry of CaCTAQ was optimized at MO6/6-31+G∗∗. 2D and 3D images were drawn with ChemDraw and Avogadro, respectively.

2. Experimental

2.1. Reagents

tert-Butyl bromoacetate, barium oxide, thallium(III) nitrate trihydrate, trifluoroacetic acid (TFA), 2-(cyclohexylamino)ethanesulfonic acid (CHES), 3-(cyclohexylamino)-1-propanesulfonic acid (CAPS), 4-(2-hydroxyethyl)-piperazine-1-ethanesulfonic acid (HEPES), and 2-(*N*-morpholino)ethanesulfonic acid (MES) were purchased from Aldrich. Tetraethyl ammonium hydroxide (TEAOH) (20 wt% in aqueous solution) was obtained from Acros Organics. Calix[4]arene was procured from Janssen and used without further purification. Chloride salts of metal ions were obtained from Aldrich. All aqueous solutions were prepared using deionized water purified in a Nano Pure System (Barnsted). Column chromatography was performed using silica gel 60 (230-400 mesh, ASTM, Merck). (Caution: Thallium salts are toxic and must be handled with care.)

2.2. Synthesis

CTAQ was synthesized according to procedures previously reported (Fig. 2-1)[32]. Tri-*tert*-butyl-calix[4]arene **2** was obtained by selective trialkylation of

calix[4]arene **1** using *tert*-butyl bromoacetate and BaO in *N,N*-dimethylformamide (DMF). The phenol moiety of **2** was oxidized to quinone using thallium(III) nitrate trihydrate in methanol and chloroform mixture (1:1, v/v). Finally, CTAQ **4** was prepared by hydrolysis of the tri-*tert*-butyl ester monoquin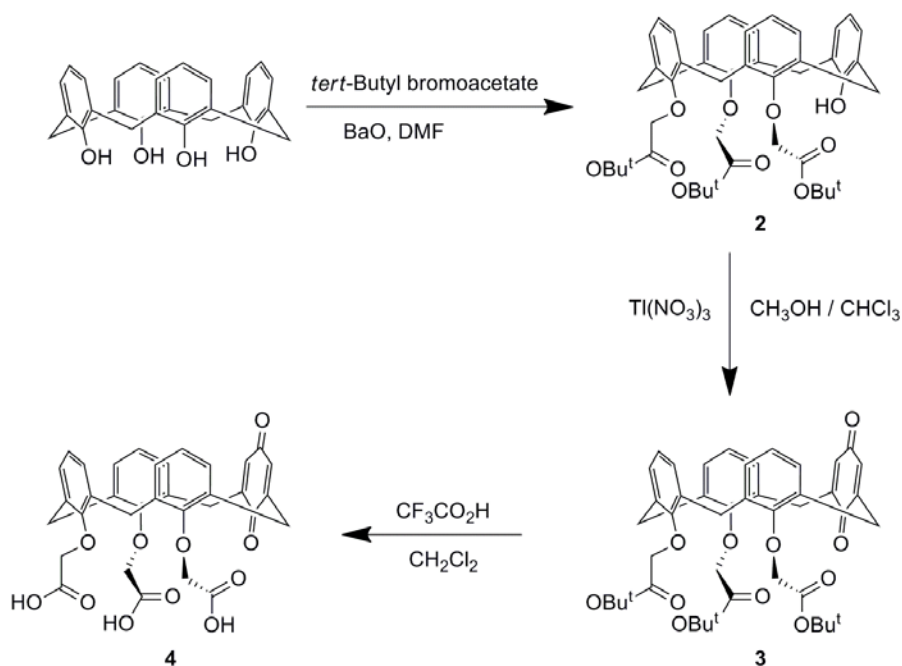one derivative **3** using TFA in dichloromethane. CTAQ is moderately soluble in basic aqueous solution, acetone, and methanol.

Fig. 2-1 Synthesis of CTAQ[32].

2.3. Electrochemistry

Electrochemical experiments were performed using a windows-driven electrochemical analyzer (CH Instruments model 660A). The surface of the glassy carbon working electrode (3 mm dia., BAS) was polished with 0.3 μm and 0.05 μm alumina (Buehler, Lake Bluff). An Ag/AgCl (in 3 M NaCl, 0.209 V vs. NHE) reference electrode and a platinum wire counter electrode were used for voltammetric experiments. Buffered aqueous solutions with pH values of 5.7, 6.2, 6.6, 7.0, 7.4, 7.8, 8.2, 8.6, 9.0, 9.4, 9.8, 10.2, 10.6, 11.0, and 11.4 contained 0.1 M of MES buffer (pH 5.7, 6.2, 6.6), HEPES buffer (pH 7.0, 7.4, 7.8, 8.2), CHES buffer (pH 8.6, 9.0, 9.4, 9.8), and CAPS buffer (pH 10.2, 10.6, 11.0, 11.4). The pH values of the buffer solutions used in the experiment were adjusted by adding hydrochloric acid (HCl) solution or TEAOH solution. Stock solutions of metal ions added to CTAQ solutions were in the form of 50 mM chloride salt. Ultrapure N_2 gas was bubbled through the solutions in all electrochemical experiments. All experiments were carried out at ambient temperature. Digital simulations of cyclic voltammograms were performed using the software package DigiElch - Professional (version 7.FD) purchased from Gamry Instruments.

2.4. Spectroelectrochemistry

All absorption UV-visible spectra were obtained with a Cary 60 UV-Vis spectrophotometer (Agilent). A SEC-C05 thin layer quartz glass spectroelectrochemical cell (ALS, path length 0.5 mm) with a Teflon cap contained the solution and electrodes. A SEC-C gauze working electrode (ALS) was used along with an Ag/AgCl reference electrode and a Pt wire counter electrode. Spectra were recorded every 6 seconds during electrolytic reduction. Solution was purged with ultrapure N_2 prior to electrolysis.

2.5. Electron Paramagnetic resonance

The model JES-TE200 (JEOL) operating at X-band (9.4 GHz) and employing 100 kHz modulation was used. Solution at pH 7.4 containing 1.0 mM CTAQ and one-equivalent of Ca^{2+} was bulk electrolyzed under ultrapure N_2 purging for 700 seconds at -0.6 V (vs. Ag/AgCl) utilizing Pt as working and counter electrodes. The solution was transferred to a flat cell and EPR spectrum was recorded after 18 minutes from the end of electrolysis. Electrolysis and EPR measurement were conducted at ambient temperature.

2.6. DFT calculation

All of the geometries of the free CTAQ and metal ion bound CTAQ (MCTAQ) were optimized at the DFT level of theory (M06 hybrid-meta functional[39]) together with LANL2DZ effective core potential (ECP)[40] for Sr and Ba atoms and $6-31+G**$ basis set for the other atoms. MO6 functional is well known to exhibit good performance on various systems such as main group thermochemistry, kinetics, organometallics and especially non-covalent interaction[39]. In addition, we employed diffuse function basis set for better description of non-covalent interactions between guest metal ion and carboxylic oxygen atoms and hydrogen bonding between the carboxylic acid groups[41]. All calculations were carried out using a suite of Gaussian 09 software packages[42].

3. Results and Discussion

3.1. Electrochemical Behavior of CTAQ and CaCTAQ

3.1.1. Cyclic voltammograms

The cyclic voltammograms of quinones in buffered aqueous solutions, in general, show a quasi-reversible pair of redox waves with relatively large peak-to-peak separation. Attributed to the coupled transfer of protons, this is what we see for CTAQ (Fig. 3-1, black curves). The only redox-active moiety of CTAQ is the quinone in the potential window employed. Therefore, CTAQ undergoes two-electron/two-proton redox reaction like a simple p-quinone, though the details of its reaction may be affected by the pendant carboxylic acid groups, as will be discussed later.

When one-equivalent of Ca^{2+} was added to CTAQ solution, however, the voltammogram was completely transformed both in neutral and basic solutions (Fig. 3-1, red curves). Acidic condition was avoided as CTAQ molecules became protonated and precipitated. First, at pH 7.4, peak-to-peak separation was drastically reduced from ~400 mV to ~80 mV and sharp, symmetric peaks appeared in both cathodic and

anodic scans. At pH 10.2, even more surprisingly, the single two-electron wave of CTAQ is split into two peaks as observed in aprotic solvents, strongly implying that sequential one-electron transfers occur.
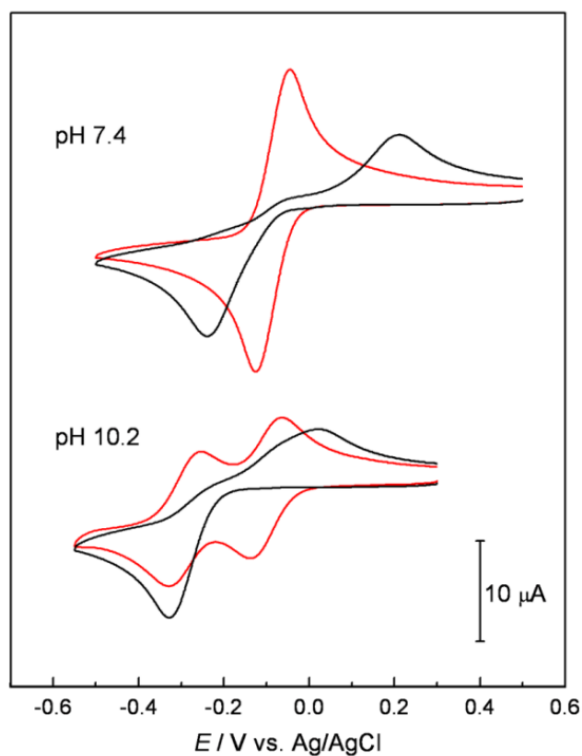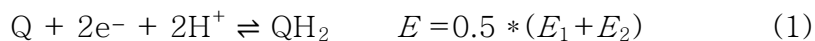

Fig. 3-1 Cyclic voltammograms of (black) CTAQ and (red) CaCTAQ at pH 7.4 and 10.2. Scan rate was 50 mV s^{-1}.

In order to clarify the electrochemical behavior of CaCTAQ, cyclic voltammetry was carried out at various pHs ranging from slightly acidic to basic and midpoint potentials (E_m)

were plotted against pH (Fig. 3-2, see Fig. 3-3 for the actual voltammograms). E_m simply indicates the average of cathodic and anodic peak potentials and roughly corresponds to the standard reduction potentials for the redox couple involved. The resulting diagram showed a remarkably systematic variation of E with pH, and redox reactions of CaCTAQ could be inferred from it (see eqs 1 ~ 3 below). In the low pH region, E_m decreased with increasing pH at a slope close to -59 mV/pH, as it should for two-electron/two-proton transfer. The single peak at low pH splits into two at higher pH, beginning at around pH 8.6. In the high pH region, the first peak remained nearly constant whereas the second peak decreased with a slope of about -59 mV/pH. E-pH diagram with superimposed lines of these slopes is shown in Fig. 3-13. Presuming that each peak involves sequential one-electron transfer, the pH-independent first peak should involve only one-electron transfer without proton transfer, whereas the second should involve one-electron/one-proton transfer. Such interpretation of the E-pH diagram is summarized below. E_1 and E_2 each designate the standard potentials for the first and second one-electron

reduction at each pH, i.e. $E_1 = E_{Q/Q^{\bullet-}}$ and $E_2 = E_{Q^{\bullet-}/QH2}$ or $E_{Q^{\bullet-}/QH-}$ or an intermediate value, depending on the pH.

pH < 8.6

$$Q + 2e^- + 2H^+ \rightleftharpoons QH_2 \qquad E = 0.5 * (E_1 + E_2) \qquad (1)$$

pH > 8.6

$$Q + e^- \rightleftharpoons Q^{\bullet-} \qquad\qquad E_1 \qquad\qquad (2)$$

$$Q^{\bullet-} + e^- + H^+ \rightleftharpoons QH^- \qquad\qquad E_2 \qquad\qquad (3)$$
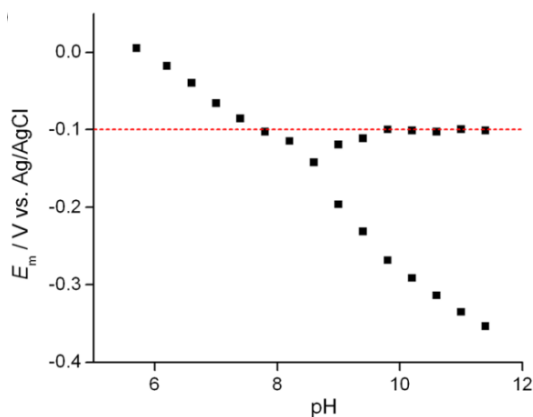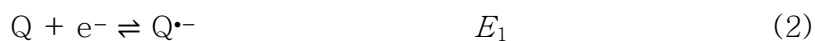

Fig. 3-2 The pH dependence of the midpoint potentials (E_m) of CaCTAQ. Midpoint potentials were obtained from cyclic voltammograms of 1.0 mM CTAQ solution in the presence of one-equivalent of Ca^{2+} (Fig. 3-3). Around the branching point (8.2 < pH < 9.0), the close distance between peaks hindered accurate determination of E_m from cyclic voltammograms.
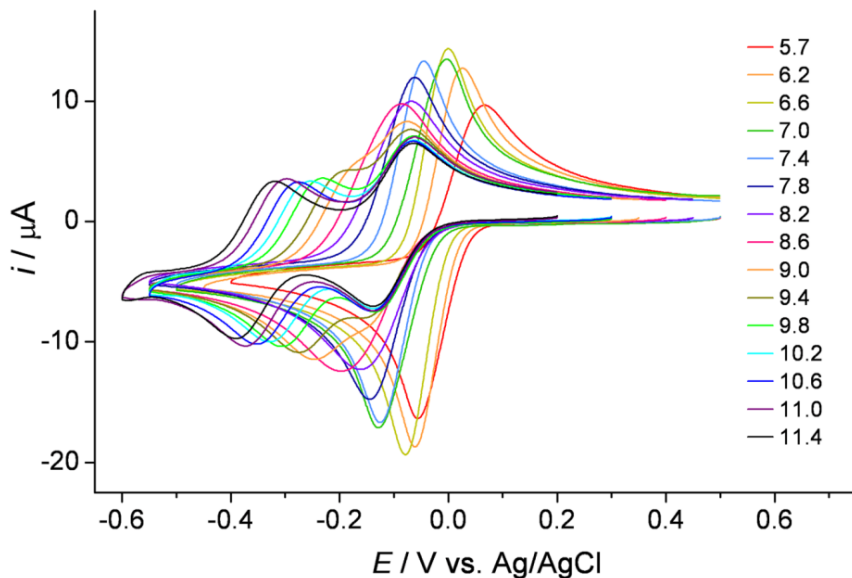
Fig. 3-3 Cyclic voltammograms of CTAQ in the presence of one-equivalent of Ca^{2+} obtained in buffered solutions at various pH values. The buffering agents were: from pH 5.7 to 6.6, MES; from pH 7.0 to 8.2, HEPES; from pH 8.2 to 9.4, CHES; from pH 10.2 to 11.4, CAPS. Concentration of CTAQ was 1.0 mM. Scan rate was 50 mV s^{-1}.

3.1.2. Confirmation of mechanism with UME

It should be noted that, as mentioned earlier, such a clear separation of the two redox steps for quinones in aqueous solutions is highly unusual. Due to the remarkable stabilization of the reduced quinone by protonation, the second electron transfer mostly follows the first reduction immediately and

produces a single two-electron peak. Even in the absence of protonation, strong hydrogen bonding of water molecules disallows the separation of the two redox steps[10].

In fact, the appearance of two peaks in itself does not guarantee sequential one-electron transfers. In unbuffered solutions at a pH where proton concentration is comparable to that of the quinone, two peaks were observed and it was once interpreted as separate one-electron transfers[43]. But it was later revealed that the two peaks each corresponded to two-electron reductions with different fates of the reduced species, namely protonation (QH_2) or stabilization by hydrogen bonding ($Q^{2-} \cdots (H_2O)_n$)[10]. It is also possible to conceive an alternative interpretation of Fig. 3-2, assigning the pH-independent peak at -0.1 V to hydrogen-bond stabilized two-electron transfer and the other peak with a slope of -59 mV/pH to two-electron/two-proton transfer. However, for CaCTAQ, we confirmed the number of electrons transferred with chronoamperometry, and the results of section 3.2 supports the extraordinary one-electron scheme as well.

We conducted chronoamperometry experiments with a Pt UME (ultramicroelectrode). At pH 10.2, step potentials that

correspond to Q•⁻, QH⁻ generation and Q re-generation according to cyclic voltammetry results were applied consecutively (Fig. 3-4). Whereas electrochemical current falls to zero after sufficient time at a conventional macroelectrode, being limited by the diffusional supply of reactants, a finite steady-state current exists at a UME because of spherical diffusion and very small electrode area. At steady state, a net diffusional flux of reactant molecules is at balance with the reaction rate at the surface of the UME. The steady-state current (i_{ss}) at a disk UME[44] is simply proportional to n, the number of electrons transferred per each reactant molecule. F is Faraday's constant (96485 C/mol), D and C^* are the diffusion coefficient and the bulk concentration of the reactant, respectively, and r is the radius of the UME.

$$i_{ss} = 4nFDC^*r \qquad (4)$$

First, the potential was stepped to a value between E_1 and E_2, intended for Q•⁻ generation. Then, when the potential was made sufficiently negative to allow full reduction, the steady-state current doubled. The steady-state current halved upon lowering the potential back to below E_2, and fell to zero when the potential returned to its initial value. According to eq

4, such variation of i_{ss} with potential is a clear indication of distinct one－electron transfers separated in potential, assuming nearly identical diffusion coefficients for Q, Q$^{•-}$ and QH$^-$ forms of CaCTAQ. It is valid to assume similar diffusion coefficients as the quinone moiety undergoing reaction is only a small portion of the large calixquinone molecule.
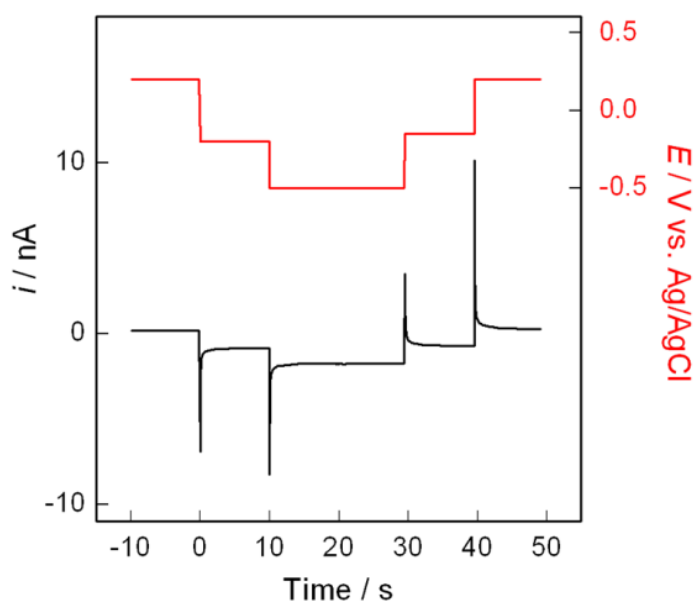

Fig. 3－4 Multi potential step chronoamperometry at a Pt UME (25 μm dia.) in 1.0 mM CTAQ solution buffered at pH 10.2 with one－equivalent of Ca^{2+} added. Red line indicates applied step potentials.

3.1.3. Influence of other metal cations

Incidentally, the influence of other redox−inactive metal cations was also investigated. Other alkaline earth metal ions showed similar trends with different degree of influence increasing in the order of $Mg^{2+} < Ba^{2+} < Sr^{2+} < Ca^{2+}$ (Fig. 3−5). Metal ion binding seems reversible as sequential addition of different metal ions in the order of increasing influence shows the same behavior as that for the metal ion added last (Fig. 3−6). The cyclic voltammogram of SrCTAQ was nearly identical to that of CaCTAQ, and Ba^{2+} showed intermediate behavior. As the binding constants of Ca^{2+}, Sr^{2+} and Ba^{2+} with CTAQ are all in the 10^6 range[45], this difference may be ascribed to their different Lewis acidities. Mg^{2+} had little effect, presumably owing to tight hydration[36] that prevents effective host−guest interaction with CTAQ. Alkali metal ions (Li^+, Na^+, K^+, Rb^+, Cs^+) had little effect[32], even at >50 equivalent, though their presence in large excess affected the voltammograms of MCTAQ (M = Ca, Sr or Ba), indicating that they competitively occupy the binding pocket of CTAQ when present in large amounts. Unfortunately, biologically significant Zn^{2+} was bound
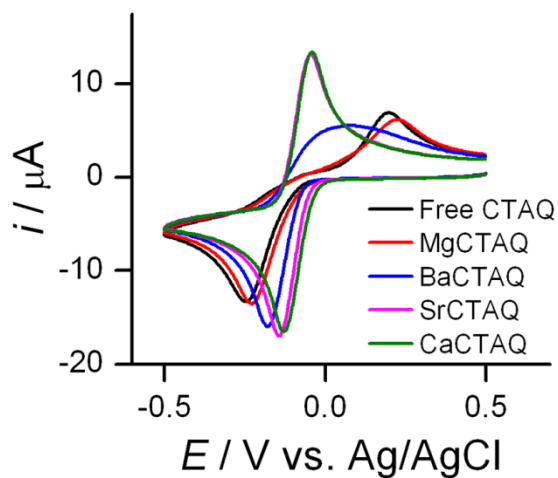
Fig. 3-5 Cyclic voltammograms of CTAQ in the presence of one-equivalent of various alkaline earth metal ions at pH 7.4. Concentration of CTAQ was 1.0 mM. Scan rate was 50 mV s^{-1}.
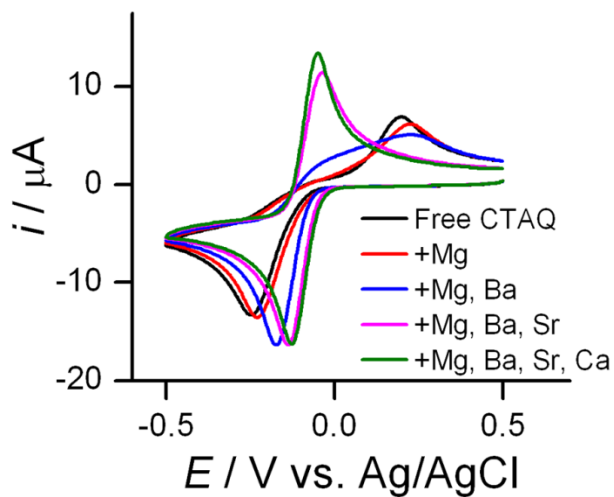

Fig. 3-6 Cyclic voltammograms of CTAQ with sequential addition of one-equivalent of various alkaline earth metal ions at pH 7.4. Concentration of CTAQ was 1.0 mM. Scan rate was 50 mV s^{-1}.

too tightly and formed precipitates with CTAQ. Therefore, we focused our attention on CaCTAQ in this study.

3.2. Stabilization of semiquinone radical anion by Ca^{2+}

3.2.1. Calculation of semiquinone stability

Separation of the one-electron reductions of quinone implies that the intermediate semiquinone is stable. The stability of the semiquinone radical anion, $Q^{\bullet-}$, can be quantitatively expressed by the equilibrium constant for the disproportionation/comproportionation reaction (eq 5), which is kinetically very facile for quinones[46]. K_{disp} is related to the rate of hydroquinone autoxidation by O_2 and superoxide production in biological systems and thus has been of much interest[3],[6]. In the literature, K_{disp} values for various quinones in aqueous solutions were estimated from the equilibrium concentration of $Q^{\bullet-}$ determined by EPR[5],[47]. However, for CaCTAQ, the separation of E_1 and E_2 at basic pH allows direct calculation of K_{disp} from electrochemical data.

The disproportionation reaction for CaCTAQ in the basic region above pH 8.6 can be written as below, involving one proton.

$$2Q^{\bullet-} + H^+ \rightleftharpoons Q + QH^- \qquad\qquad K_{disp1} \qquad\qquad (5)$$

Because of the involvement of one proton, K_{disp1} is a function of pH. A modified parameter, $K_{disp1,pH}$, can be defined as follows.

$$K_{disp1,pH} = K_{disp1}[H^+] = \frac{[QH^-][Q]}{[Q^{\bullet-}]^2} \qquad\qquad (6)$$

$$\log K_{disp1,pH} = -pH + \log K_{disp1} \qquad\qquad (7)$$

Simple derivation with the Nernst equation gives eq 10 from eqs 6, 8 and 9.

$$E = E_{Q/Q^{\bullet-}} + \frac{RT}{F}\ln\frac{[Q]}{[Q^{\bullet}]} \qquad\qquad (8)$$

$$E = E_{Q^{\bullet-}/QH-} + \frac{RT}{F}\ln\frac{[Q^{\bullet}][H^+]}{[QH^-]}$$

$$= E_{Q^{\bullet-}/QH-,pH} + \frac{RT}{F}\ln\frac{[Q^{\bullet}]}{[QH^-]} \qquad\qquad (9)$$

$$\log K_{disp1,pH} = \frac{F}{2.303RT}(E_{Q^{\bullet-}/QH-,pH} - E_{Q/Q^{\bullet-}}) \qquad (10)$$

Because $E_{Q/Q^{\bullet-}}$ and $E_{Q^{\bullet-}/QH-,pH}$ equals E_1 and E_2 at each pH in the basic region, $\log K_{disp1,pH}$ could be plotted against pH to give a linear plot (Fig. 3−7) using the data in Fig. 3−2. The slope of −1.07 was in good agreement with eq 6. Extrapolating to neutral pH, $K_{disp1,pH}$ was estimated to be $10^{-0.1}$, or 0.8, at pH

7.4. Considering the fact that the major reduced species at pH 7.4 is QH_2, and assuming $pK_{a,QH-/QH2}$ to be 8.6, the effective disproportionation constant at pH 7.4 was calculated to be $10^{1.1}$, or 13. (note: Eqs 1 ~ 3 suggest that $pK_{a,QH-/QH2}$ should be no larger than 8.6. Because a large pK_a value favors the right side of the equilibrium in eqs 5 and 6, K_{disp} is larger for higher pK_a value. It can be seen that even when assuming the largest plausible value of pK_a for CaCTAQ, $K_{disp,pH}$ is still very small.) This is five orders of magnitude smaller than the value of ~10^6 for 2,6-dimethyl-1,4-benzoquinone (DMBQ), which is a simple structural analog for the quinone moiety of CTAQ[5]. The value suggests that the semiquinone radical anion becomes more stable in the presence of Ca^{2+}.
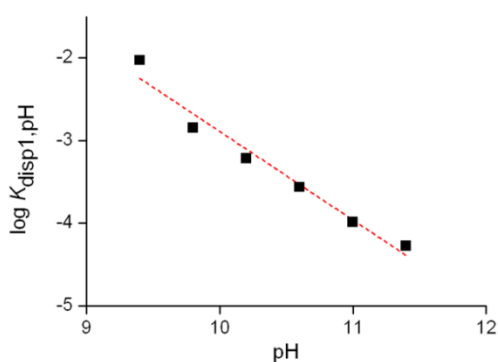

Fig. 3-7 Plot of log $K_{disp1,pH}$ against pH for CaCTAQ. The slope is −1.07 ($R^2 = 0.96$).

3.2.2. Spectroscopic verification

The conclusion that CaCTAQ$^{\bullet-}$ is very stable even at pH 7.4 called for spectroscopic verification of this species. While cyclic voltammetry at neutral pH was inherently unable to confirm their existence, spectroelectrochemical experiment utilizing optically transparent thin layer electrochemical (OTTLE) cells[48] was expected to reveal the existence of Q$^{\bullet-}$ produced via comproportionation. Bulk electrolysis in neutral solution at a fixed potential was performed along with simultaneous observation of the UV－Vis spectra.

The UV－Vis absorption spectra in Fig. 3－8 demonstrate the concentration changes of various species of CTAQ and CaCTAQ during electrolysis. In the absence of Ca^{2+} ion (Fig. 3－8a), the appearance of clear isosbestic points implied that no intermediate species was present. The absorption peak at 256 nm rapidly decayed while the peak at 300 nm kept increasing during electrolysis. These two peaks were assigned to CTAQ and CTAQH$_2$, respectively, as their wavelengths were similar to those of 1,4－benzoquinone (BQ) and BQH$_2$ in the literature, which are 246 and 289 nm[49].
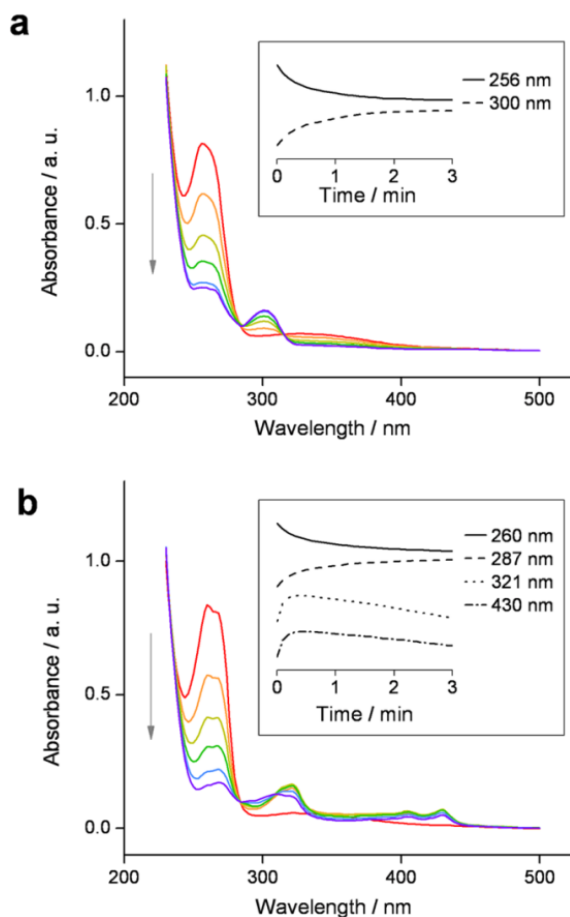
Fig. 3-8 UV-visible absorption spectra obtained during electrochemical reduction of CTAQ in the (a) absence and (b) presence of one-equivalent of Ca^{2+} in pH 7.4 buffered solutions. Spectra are shown for 0, 12, 30, 60, 120, 180 s after the onset of electrolysis, in the order indicated by the arrow (i.e., from red to purple). (Inset) Time-dependent absorbance profiles at different wavelengths. The absorbance values were normalized for ease of comparison. Concentration of CTAQ = 1.0 mM. Applied potential = −0.6 V vs. Ag/AgCl.

In the presence of one-equivalent of Ca^{2+} ion (Fig. 3-8b), the absorption peak at 260 nm decreased in a similar way to the 256 nm peak of CTAQ, suggesting that the peak at 260 nm can be assigned to the unreduced CaCTAQ. However, unlike CTAQ, the isosbestic point above 300 nm was blurred and new peaks emerged at 321, 405 and 430 nm. These new peaks rose and fell during electrolysis, implying that these peaks represented intermediate species with a significantly long lifetime. The only plausible intermediate species in CaCTAQ reduction is the semiquinone radical anion, $CaCTAQ^{\bullet-}$. Moreover, these wavelengths were close to where those for the semiquinone radical anion of BQ reportedly appeared (~315 and ~430 nm)[49],[50]. Because the electrode reaction produces the fully reduced $CaCTAQH_2$, the semiquinone radical anion, $Q^{\bullet-}$, must have come from comproportionation between CaCTAQ and $CaCTAQH_2$. The peak representing $CaCTAQH_2$ seemed to overlap with that of $CaCTAQ^{\bullet-}$ at 300 nm, but a small peak at 287 nm could be picked out and assigned to $CaCTAQH_2$ only, judging from its monotonous increase throughout the electrolysis. Hence, UV/Vis spectra recorded during

potentiostatic reduction of CTAQ and CaCTAQ imply that semiquinone becomes very stable in the presence of Ca^{2+}.

For added proof, the radical character of the transient species in UV-Vis spectra was confirmed by EPR. The bulk-electrolyzed CaCTAQ solution showed a very strong and clear EPR signal that slowly decayed with time and was similar to that of BQ$^{•-}$ (Fig. 3-9) [50],[51]. Incidentally, an EPR signal was observed in the case of free CTAQ (not shown) as well but was far weaker in strength and barely resolved.
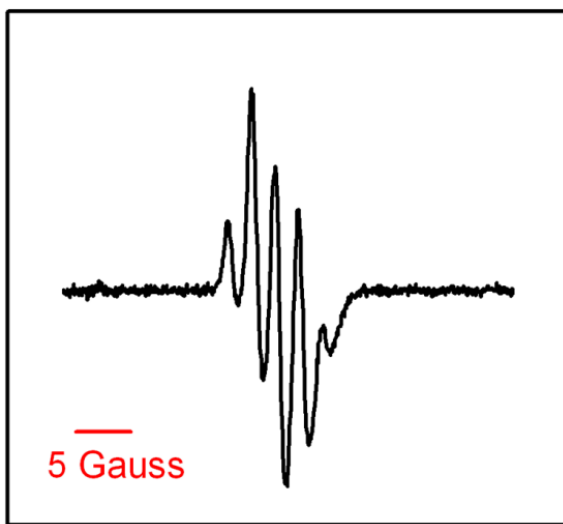
Fig. 3-9 EPR spectrum of bulk-electrolyzed CaCTAQ recorded after 18 minutes from the end of electrolysis.

3.3. Digital simulation of cyclic voltammograms of CaCTAQ

3.3.1. Simulation procedure

The preceding sections revealed the unusual redox mechanism and semiquinone radical stability of CaCTAQ by investigating the cyclic voltammograms obtained at various pHs. Digital simulation of CaCTAQ voltammograms was performed in order to corroborate the proposed mechanism and obtain additional quantitative information. Fig. 3-10 summarizes the mechanism employed in the simulation. Full tabulation of all the reactions and associated parameters is provided in Table 3-1.

Considering the low pK_a of semiquinones, e.g. below 5 for DMBQ, the protonated neutral semiquinone radical, QH•, was expected to participate little in the pH region investigated. Moreover, the complexation of Ca^{2+} is expected to lower the pK_a of QH• further. Thus, the contribution of QH• was neglected in the simulation after verifying its incorporation had little effect for reasonable pK_a values. For the second electron transfer, which is a PCET, including a concerted proton-electron transfer (CPET) pathway enabled us to better reproduce the experimental voltammogram, in line with several
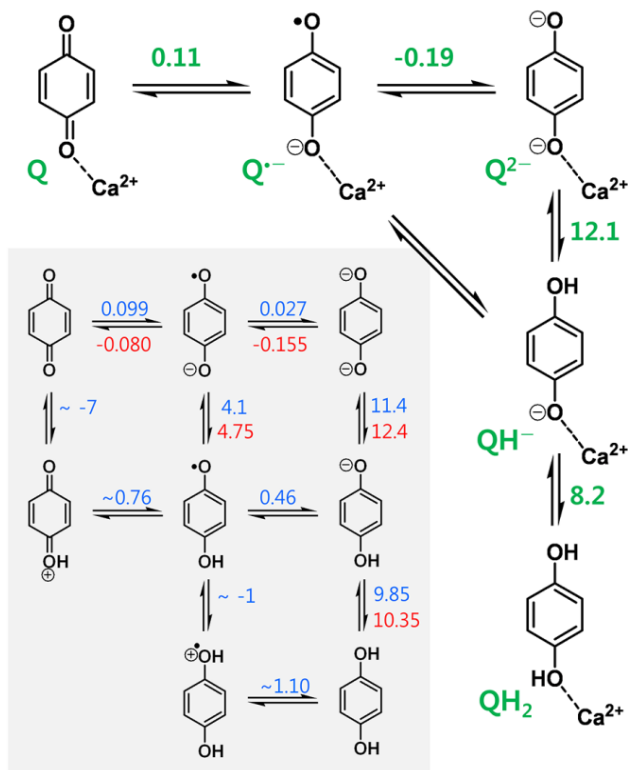
Fig. 3-10 Digital simulation and analogous schemes for BQ and DMBQ. Numbers indicate E (V vs. NHE) and pK_a values for (Outer, green) CaCTAQ, (inner, blue) BQ and (inner, red) DMBQ, which were obtained from simulation for CaCTAQ and from literature for BQ[55] and DMBQ[6],[56],[57]. (note: some of these values are not directly obtained but calculated from other E and pK_a. Also, slightly different values were previously reported in the literature[5],[58].)

recent reports on CPET[38],[52]-[54]. When modeling protonation steps, both specific and general acid catalysis were considered by using two reaction equations for each protonation reaction, one involving H^+ (equivalent to H_3O^+) and the other involving the acid form of the buffer species. The pH was set by adjusting the concentrations of the acid and base forms of the buffer.

Diffusion coefficient for CaCTAQ and its reduced forms was estimated from chronoamperometric currents recorded at a UME (Fig. 3-4). The transient decay of current at a potential step of −0.2 V was analyzed according to an established methodology[59]. The diffusion coefficient (D) of CaCTAQ was estimated to be 2.4×10^{-6} cm^2 s^{-1} from the slope of $i(t)/i_{ss}$ vs. $t^{-1/2}$ plot, which was obtained using the following equation (Fig. 3-11). The diameter of UME was calibrated by an equivalent analysis of the steady-state current of 2.0 mM ferrocene in acetonitrile, 0.1 M tetrabutylammonium perchlorate solution, referring to its diffusion coefficient of 2.3×10^{-5} cm^2 s^{-1} in the literature[60].

$$\frac{i(t)}{i_{ss}} = 0.7854 + \frac{r\sqrt{\pi}}{4\sqrt{Dt}} \qquad (11)$$

Incidentally, after determining D, the number of electrons transferred (n) could be calculated using eq 4. The calculated n value was 1.1, roughly equal to 1, again confirming the extraordinary one-electron reduction behavior of CaCTAQ.
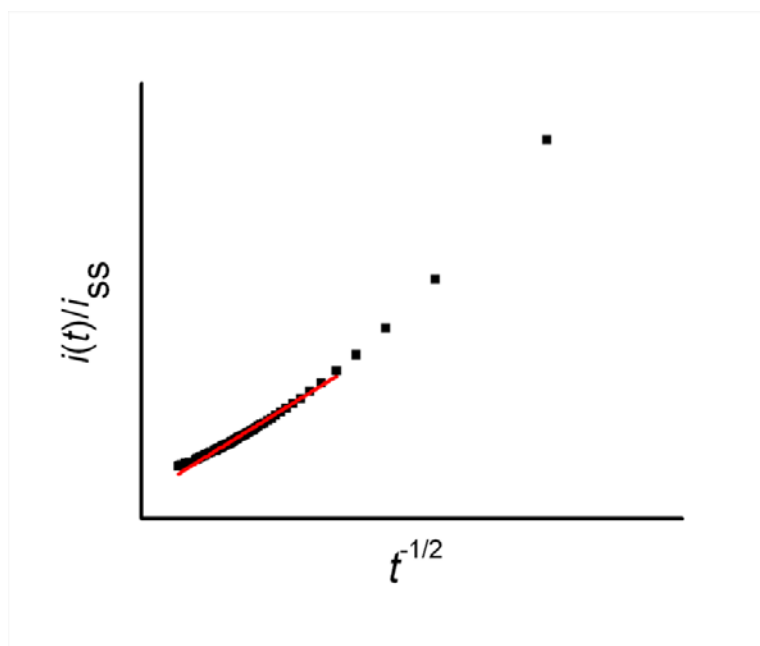
Fig. 3-11 Plot of the current ratio $i(t)/i_{ss}$ against the inverse square root of time for the reduction of CTAQ in the presence of one-equivalent of Ca^{2+} in pH 10.2 buffered solution. The chronoamperometry experiment was performed at a platinum UME (25 □m dia.) by stepping the potential from a value where no current flows (0.2 V) to a value corresponding to one-electron reduction (–0.2 V) (Fig. 3-4). y-intercept 0.7854, slope –0.337, R^2=0.99.

The values of the standard reduction potentials, acid dissociation constants and various unknown rate constants were determined by fitting the simulated voltammograms to the experimental data. As a rule, all protonation reactions were given a diffusion-limited rate[61] and disproportionation reaction rates were set by referring to the literature[46]. Applying an identical set of parameters to pH values ranging from 7.0 to 11.4 allowed us to narrow down the uncertainty in the obtained parameters. In fact, it is normally difficult to unambiguously simulate voltammograms of multiple electron transfers coupled to proton transfers because of the large number of unknown parameters involved, even if pH or scan rate is varied to check the validity of the simulation[38],[62]. However, for CaCTAQ, the separation of two-electron redox wave into one-electron waves at high pH enabled relatively straightforward simulation. E for the Q/Q$^{\bullet-}$ couple (E_1) was already evident from Fig. 3-2, and p$K_{a,QH-/QH2}$ could be roughly estimated *a priori* as well, as discussed previously. Initial guesses of other E and pK_a values were taken from those of DMBQ. As for estimating the individual heterogeneous rate constants, for which wildly disparate estimations exist in the

Table 3-1 The full mechanism employed in digital simulation of cyclic voltammograms.

Electron transfer reactions[a] (ET: electron transfer, CPET: concerted proton-electron transfer)

	Reaction	E^0 (V vs. Ag/AgCl)	k_s (cm s^{-1})
ET	$Q + e^- \rightleftharpoons Q^{\bullet-}$	−0.10	0.005
	$Q^{\bullet-} + e^- \rightleftharpoons Q^{2-}$	−0.40	0.005
CPET	$Q^{\bullet-} + BH + e^- \rightleftharpoons QH^- + B^-$	(depends on buffer) [b]	0.10

Chemical reactions (PT: proton transfer, DISP: disproportionation)

	Reaction	K_{eq}	k_f (M^{-1} s^{-1})
PT	$Q^{2-} + H^+ \rightleftharpoons QH^-$	1.2×10^{12}	1×10^{10}
	$Q^{2-} + BH \rightleftharpoons QH^- + B^-$	(depends on buffer) [b]	
	$QH^- + H^+ \rightleftharpoons QH_2$	1.5×10^{8}	
	$QH^- + BH \rightleftharpoons QH_2 + B^-$	(depends on buffer) [b]	
DISP	$Q^{\bullet-} + Q^{\bullet-} \rightleftharpoons Q + Q^{2-}$	8.5091×10^{-6} [b]	1×10^{8}
Acid-base equilibria	$B^- + H^+ \rightleftharpoons BH$	3.02×10^{7} for HEPES 2.00×10^{9} for CHES 2.51×10^{10} for CAPS	1×10^{10}
	$H^+ + OH^- \rightleftharpoons H_2O$	5.5×10^{15}	

a: All α values were assumed to be 0.5.

b: Thermodynamically superfluous reactions (TSR). Their E^0 (or K_{eq}) values were determined by other E^0 (or K_{eq}) values and automatically entered by the simulation software.

literature, the wave separation at basic pH again helped. The ET rate constant for Q/Q$^{\bullet-}$, as it was a simple one−electron transfer, could be estimated directly by fitting. For the second ET, the concerted pathway was predominant so that k_{CPET} could also be directly estimated by fitting. The ET rate constant for Q$^{\bullet-}$/Q^{2-} mattered little for reasonable values of k_{ET}, and was assumed to be the same as the k_{ET} for the first ET. Although plausible values were obtained for rate constants in this way, we do not claim these rate constants to be accurate values, but rather focus on discussing the implications of the thermodynamic parameters.

3.3.2. Simulation results

As shown in Fig. 3−12, good fit was achieved over the pH range employed. The peak potentials were well reproduced and shapes of the cyclic voltammograms were similar in general. A small difference in the peak currents might be due to limited accuracy in the estimation of the diffusion coefficient. The Pourbaix diagram constructed from simulation results and overlaid over experimental data is given in Fig. 3−13. The good correlation overall again supports the validity of the proposed mechanism. Only the region between pH 5.7 and 6.6, where
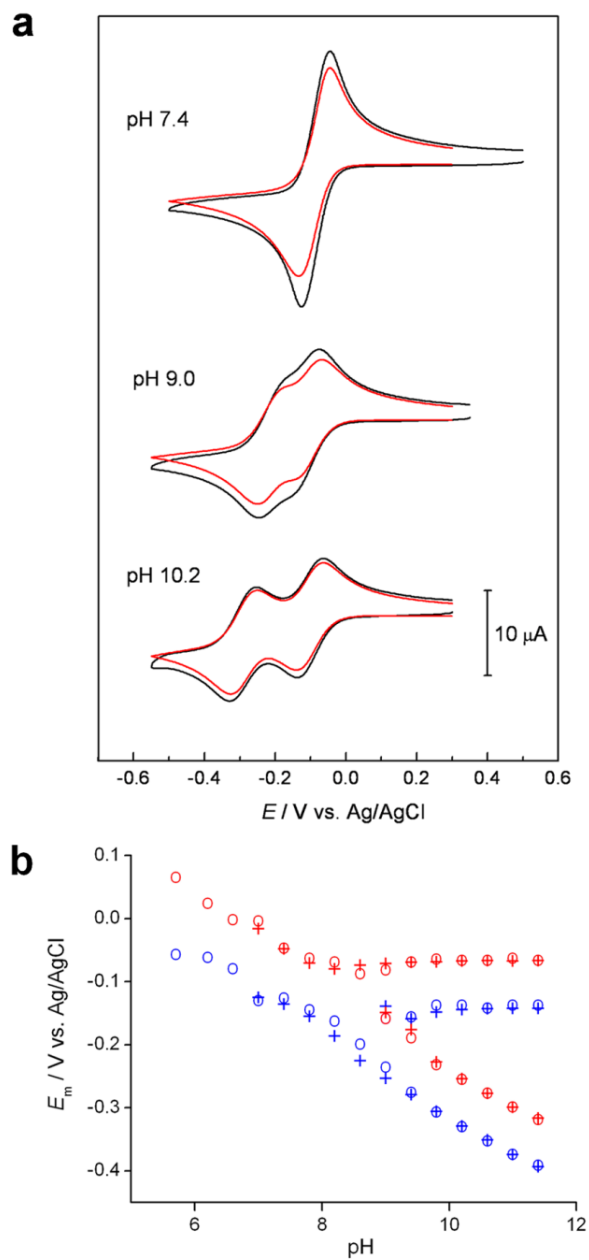
Fig. 3-12. (a) (Red) Simulated and (black) experimental cyclic voltammograms of CaCTAQ. (b) (Red) Cathodic and (blue) anodic peak potentials of (+) simulated and (O) experimental voltammograms.
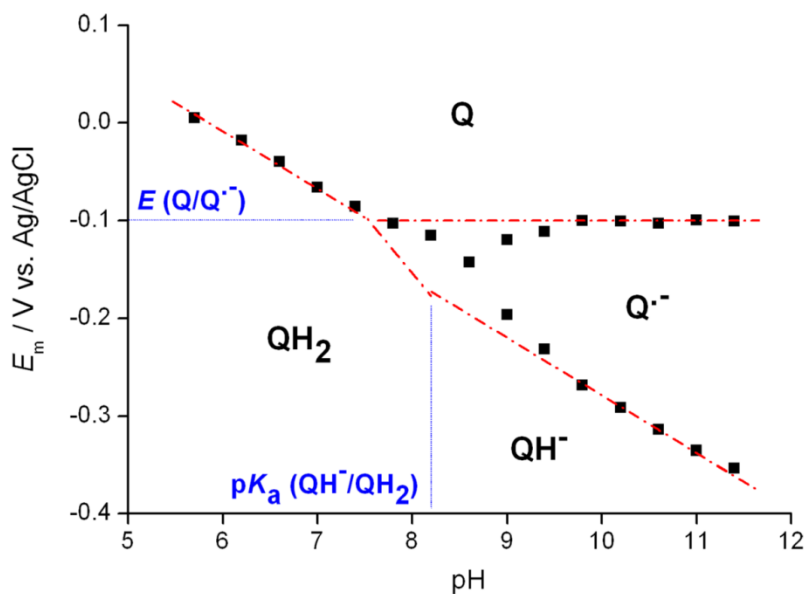
Fig. 3-13 E-pH diagram of CaCTAQ with boundaries added to show the dominant quinone species in different areas. E and pK_a values are from simulation. Dots are experimental data. The slopes of dash-dot lines are −59, −118, −59 mV/pH from left to right. Around the branching point (8.2 < pH < 9.0) where the points deviate from the lines, the close distance between peaks hindered accurate determination of E_m.

MES buffer was employed, did not show good agreement between experimental and simulated voltammograms. The protonated semiquinone, QH•, might have begun to appear in considerable amount at this low pH; or metal ion complexation

could have become weaker, as Ca^{2+} is known to be released from complexes in acidic condition[37].

Now with the results of simulation at hand, we can compare Ca^{2+}-complexed quinone with free quinone in terms of thermodynamic parameters. For the sake of comparison with CaCTAQ, it was deemed appropriate to take the E and pK_a values of DMBQ to represent those of Ca^{2+}-free quinone, on the basis of structural similarity and the fact that complexation of Ca^{2+} precludes the participation of carboxylic acid groups in the PCET of quinone. (note: Simulation of CTAQ, which possesses three pendant carboxylic acid groups, was a formidable task; experimental E-pH diagram of CTAQ showed a slope of -50 mV/pH throughout the pH range investigated, slightly deviating from the theoretical value of -59 mV/pH, and simulation with the simple scheme used for CaCTAQ did not work and implied the participation of intramolecular acid-base equilibria, namely those of the pendant carboxylic acid groups.) According to Fig. 3-10, $E_{Q/Q^{\bullet-}}$ becomes more positive and $E_{Q^{\bullet-}/Q^{2-}}$ more negative in the presence of Ca^{2+}. Also, $pK_{a,QH-/QH2}$ is two orders of magnitude smaller for CaCTAQ than for DMBQ. Calculating E_2 from solution pH, E and pK_a values of QH_2 (eq

12), E_1 and E_2 were found to shift ~200 mV positively and negatively, respectively, for CaCTAQ with respect to DMBQ at pH 7.4. E_1 and E_2 at pH 10.2 were also shifted positively and negatively. In eq 10, pK_{a1} and pK_{a2} each stands for $pK_{a,QH-/QH2}$ and $pK_{a,Q2-/QH-}$.

$$E_2 = E_{Q\bullet-/Q2-} + \frac{RT}{F}\ln\frac{[H^+]^2 + [H^+]K_{a1} + K_{a1}K_{a2}}{K_{a1}K_{a2}} \qquad (12)$$

Such positive and negative shift in E_1 and E_2 comprise all the essence of the change induced by Ca^{2+}. The peak separation at basic pH is a natural result, because it is exactly the fact that E_2 is more positive than E_1, namely potential inversion, that caused the two redox waves to overlap and result in a merged, two-electron peak. Also, as demonstrated by the calculation of K_{disp}, more negative value of $E_2 - E_1$ directly translates into greater stability of the semiquinone (eq 9). Because Ca^{2+} shifts E_1 positively and E_2 negatively, it decreases the value of $E_2 - E_1$ and stabilizes the semiquinone.

Moreover, the vast difference between the voltammograms of CTAQ and CaCTAQ at neutral pH (Fig. 3-1) can be easily understood. Since the inherent ET rates of quinones are quite slow (0.005 cm s^{-1} for CaCTAQ), the onset

potentials for reduction and oxidation occur near E_1 and E_2, respectively[63]. When there is a large potential inversion, i.e. $E_2 - E_1 \gg 0$, E_1 is much more negative than the overall thermodynamic reduction potential, E_{ave}, so a significant overpotential is required to drive reduction. The same applies to oxidation, as E_2 is much more positive than E_{ave}. In the literature, this concept is contained in the apparent rate constant k_{app} for the overall two-electron redox reaction, a parameter that is determined by the individual E, pK_a values and solution pH, following the theoretical framework of Laviron[64],[65]. For interpreting voltammograms it seems more intuitive to think in terms of E_1 and E_2. As $E_2 - E_1$ decreases, i.e. there is less potential inversion, the required overpotential decreases, and the overall, apparent kinetics for the electrode reaction is enhanced. This accounts for the transformation of the voltammogram induced by Ca^{2+} at neutral pH.

3.4. Electrocatalytic reduction of CTAQ by Ca^{2+}

3.4.1. At neutral pH

The enhanced kinetics of CaCTAQ implies that in principle CaCTAQ can act as an electron mediator for CTAQ.

Because of the relative values of E_1 and E_2, if a potential sweep is carried out in a solution containing both CTAQ and CaCTAQ species, the CaCTAQ species will always be reduced and oxidized before CTAQ or CTAQH$_2$. Also, CaCTAQ and CTAQ were found to easily undergo homogeneous reactions with each other exchanging electrons and protons (eq 13), just as their comproportionation and disproportionation reactions are very facile, and similarly to other simple quinones[66]. Therefore, CTAQ will be reduced and oxidized via CaCTAQ before sufficiently high electrode potential is reached for direct electron transfer at the electrode. In other words, CTAQ will be reduced and oxidized electrocatalytically.

$$CaCTAQH_2 + CTAQ \rightleftharpoons CaCTAQ + CTAQH_2 \qquad K_{ex} \qquad (13)$$

The actual cyclic voltammograms, recorded after adding less than one-equivalent of Ca^{2+} to a solution of CTAQ at pH 7.4, are presented in Fig. 3-14a. The high binding constant of CTAQ implies that CaCTAQ mole fraction should approximately equal the equivalence of Ca^{2+} added. As explained above, catalytic currents were observed on both forward and reverse scans. On the cathodic scan, even adding as little as 0.05 equiv of Ca^{2+} was enough to pull forward the reduction peak so that it

nearly overlapped with the reduction peak for CaCTAQ. This
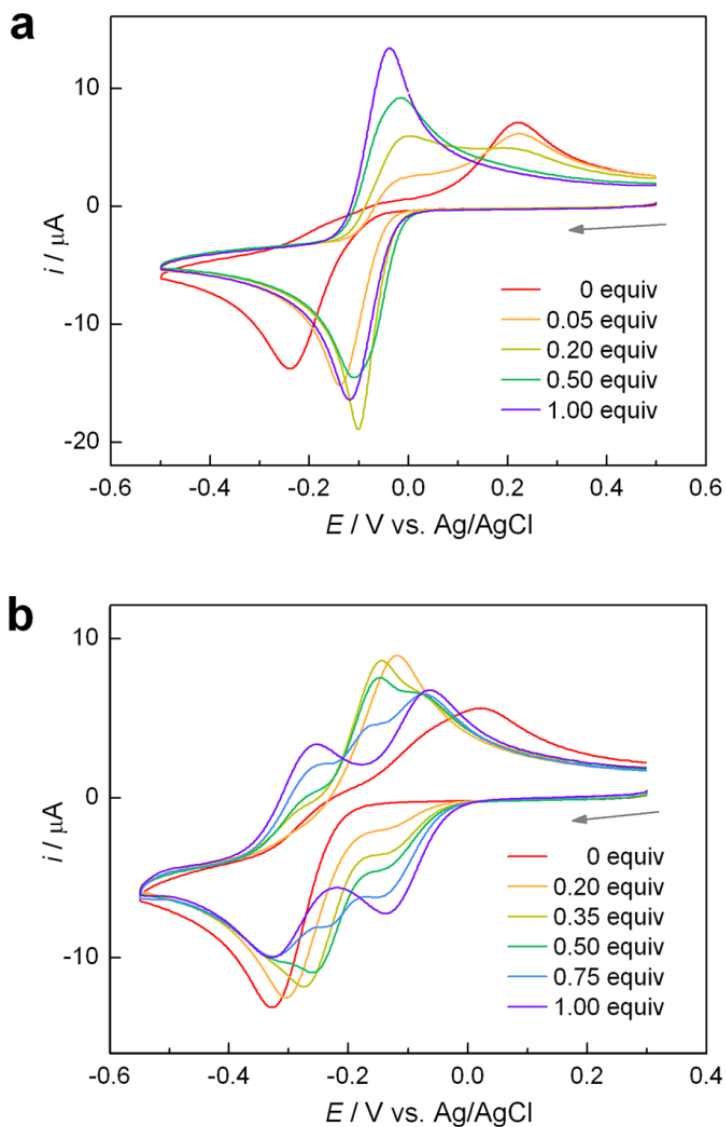indicates that CaCTAQH$_2$ generated at the electrode surface

Fig. 3-14 Cyclic voltammograms of 1.0 mM CTAQ in the
presence of various amounts of Ca^{2+} in (a) pH 7.4 or (b) pH
10.2 buffered solution. Scan rate was 50 mV s^{-1}.

rapidly reduces the free CTAQ molecules around it. Incidentally, both the peak current and peak potential implied more enhanced reduction at 0.20 equiv of Ca^{2+} than at 1 equiv. A possible explanation is that the electron relay from $CaCTAQH_2$ to CTAQ was faster than the diffusion of CaCTAQ to the electrode, so that the reduction current reached a maximum earlier when both CTAQ and CaCTAQ were present than when there were CaCTAQ only. On the anodic scan, two oxidation peaks are found that obviously correspond to Ca^{2+}-complexed and Ca^{2+}-free reduced quinones, but their relative heights did not reflect their molar ratio. For instance, at 0.20 equiv of Ca^{2+}, the peak heights were close to 1:1 rather than 1:4. This indicates that the CaCTAQ oxidized at the electrode subsequently oxidizes $CTAQH_2$ around it.

Therefore, electrocatalytic activity of CaCTAQ was found on both scan directions, but it was clearly stronger during the cathodic scan. In other words, the equilibrium of eq 13 lies more toward the right. K_{ex} being greater than 1, the direct correlation between standard reduction potentials and equilibrium constants dictates that the overall reduction

potential of CaCTAQ should be more negative than CTAQ (eqs 14 ~ 15).

$$K_{ex} = \frac{[CaCTAQ]}{[CaCTAQH_2]} \frac{[CTAQH_2]}{[CTAQ]} \qquad (14)$$

$$\ln K_{ex} = \frac{2F}{RT}(E_{ave,CaCTAQ} - E_{ave,CTAQ}) \qquad (15)$$

3.4.2. At basic pH

At pH 10.2, where wave separation occurs, the voltammograms with <1 equiv Ca^{2+} were symmetrically shaped and showed different features from those at pH 7.4 (Fig. 3-14b). A close examination on the basis of previous discussions makes the mechanism behind it clear. The initial peak in either cathodic or anodic scan grows roughly in proportion with the mole fraction of CaCTAQ and thus implies little catalytic current. It is because this peak corresponds to the one-electron reduction or oxidation of CaCTAQ or $CaCTAQH^-$, producing the semiquinone $CaCTAQ^{\cdot-}$. Its homogeneous reaction with either CTAQ or $CTAQH_2$ is unfavorable because of the high instability of the semiquinone $CTAQ^{\cdot-}$ that will be produced. The CaCTAQ species act as an electron mediator only after their two-electron transfer products are formed.

They may come from electrode reaction or disproportionation. As the mole fraction of CaCTAQ is increased, the peak for CTAQ shifts in potential so that less overpotential is required, and decreases in height at the same time. The potential shift is due to the catalytic action of CaCTAQ species, as explained for the case of neutral pH. The decrease in peak height, on the other hand, follows the decreasing mole fraction of the $Ca^{2+}-$ free quinone. This can be understood considering that unlike in neutral solution, the peaks for catalytic redox of CTAQ and heterogeneous redox of CaCTAQ are not merged. It is because the potential for the second one$-$electron reduction of CaCTAQ (E_2) is more negative than that for the two$-$electron reduction of CTAQ (E_{ave}), and CaCTAQH$^-$ required for the homogeneous reduction of CTAQ is produced via disproportionation before the electrode potential reaches E_2. Analogous reasoning can be applied to the oxidation reactions. In addition to deciphering the reactions involved in the voltammograms, it was inferred from their symmetric shape that K_{ex} is close to 1, i.e. that E_{ave} of CTAQ and CaCTAQ are similar at this pH. Assuming $E_{ave,CTAQ} = E_{ave,CaCTAQ}$ at pH 10.2, E_{ave} of CTAQ was found to be ~60 mV

more positive than the E_{ave} of DMBQ. This may be due to the stabilization of $CTAQH_2$ by the pendant carboxylate groups.

However, it is counterintuitive that E_{ave} of CaCTAQ is more negative than that of CTAQ at pH 7.4. The complexation of Ca^{2+}, a metal cation, is making it harder to reduce the quinone. It is a common sense in organic chemistry that complexation of a Lewis acid like Ca^{2+} makes the substrate electrophilic and more reducible. On the other hand, observing the color change of CTAQ solution over time implied otherwise. Nucleophilic attack by OH^- is known to occur at unsubstituted quinones[67],[68] and change the color of the quinone solution from yellow to brownish-red to violet-red[25]. Such color change was also observed with CTAQ, and its rate dramatically accelerated in the presence of Ca^{2+}; at high pH, the solution turned brownish after less than 10 minutes from adding Ca^{2+}. It is evident that Ca^{2+} renders the quinone moiety electrophilic and susceptible to nucleophilic attack by OH^-. This apparent contradiction will be resolved as we clarify the influence of Ca^{2+} in the next section.

3.5. Elucidating the role of Ca^{2+} and aqueous environment in shifting E_1 and E_2

3.5.1. Discussion based on literature survey

To summarize the results obtained so far, interesting new properties emerged when Ca^{2+} is bound to CTAQ. All of those observations are in essence results of positive and negative shift in E_1 and E_2 of the quinone. Reported many times in the literature from electrochemical and photoinduced electron transfer experiments, the positive shift of E_1 has been attributed to the Lewis acidity of Ca^{2+} and the stabilizing effect that it has on the semiquinone radical anion by electrostatic attraction. The term MCET designates this metal ion-assisted one-electron transfer to quinone. The negative shift of E_2 is a little bit less straightforward, and has appeared less frequently in the literature than the positive shift of E_1. We could only find a single case that directly reported the negative shift of E_2[24]. As for studies with less direct relevance, autoxidation of quinones by dissolved oxygen was reported to be generally enhanced by the presence of metal ions, as noted earlier[26],[27],[69]. These studies explained their observations by assigning two roles to the metal ion: promoting deprotonation of the fully reduced quinone to destabilize it and stabilizing the semiquinone radical anion.

While these explanations are valid and roughly recapitulate the role of Ca^{2+} in CaCTAQ, our case requires a little more clarification. Since CTAQ is a p-quinone, the Ca^{2+} is bound to one of the oxygens only, whereas the Ca^{2+} was dually coordinated by the quinone in previous studies, as they all dealt with o- or hydroxy-quinones. Thus, the tendency to promote deprotonation is weaker in CaCTAQ. Indeed, the pK_a of CaCTAQH$_2$ compared to DMBQH$_2$ shows that Ca^{2+} is not very effective in hindering protonation; especially the oxygen on the other side is little affected (Fig. 3-10). Moreover, not only $E_{Q^{\bullet-}/QH2}$ but also $E_{Q^{\bullet-}/Q2-}$ is more negative for CaCTAQ than DMBQ. As E for CTAQ seems to be even more positive than DMBQ (vide supra), it can be reasonably assumed that E_2 of CTAQ, both with and without protonation, became more negative by the complexation of Ca^{2+}.

As for the stabilization of Q$^{\bullet-}$ by Ca^{2+}, if it is wholly attributed to electrostatic effects, QH$^-$ and Q^{2-} should be equally stabilized by Ca^{2+} as well. However, as the thermodynamic redox potential depends on the relative stability of the reduced and oxidized forms, equal stabilization of the semiquinone and fully reduced quinone anions cannot induce a

negative shift in E_2. Some literature has referred to the seemingly extraordinary stabilization of the semiquinone radical anion by metal ions with the term "spin stabilizer"[70]. But Ca^{2+} is a diamagnetic species, and our effort to identify any physical grounds for additional stabilization of $Q^{\bullet-}$ over Q^{2-} large enough to account for the negative shift of E_2 was unsuccessful. In fact, in aprotic solvents, metal ions were shown to stabilize Q^{2-} more than $Q^{\bullet-}$[21],[71], in good accord with classic electrostatic considerations[72]. (note: Ref [71] does not directly state that Q^{2-} is more stable than $Q^{\bullet-}$ when complexed with metal ion. However, upon metal ion addition, the one−electron transfer becomes a two−electron transfer, which indicates that the positive shift of E_2 is larger than that of E_1; therefore, we can say that Q^{2-} was more stabilized than $Q^{\bullet-}$.)

Therefore, we rather attributed the extra stabilization of semiquinone or destabilization of fully reduced quinone by Ca^{2+} to the aqueous environment surrounding CaCTAQ and CTAQ. Survey of the literature on quinone electrochemistry indicates that the stabilizing effect of hydrogen bonding is weaker upon the semiquinone than upon the fully reduced quinone. In aprotic solvents, quinones show two clearly separated one−electron

waves, which move toward positive potential upon incremental addition of hydrogen bonding agents such as water[9]. The two waves eventually overlap because the second wave corresponding to $Q^{\bullet-} \rightarrow Q^{2-}$ moves much more rapidly than the first wave corresponding to $Q \rightarrow Q^{\bullet-}$. Actually, the first wave is scarcely shifted, indicating that $Q^{\bullet-}$ is much less stabilized by hydrogen bonding. Electrochemical study of quinones in unbuffered aqueous solutions also reported stronger hydrogen bonds formed on Q^{2-} than on $Q^{\bullet-}$[10]. Intramolecular hydrogen bonding is known to stabilize $Q^{\bullet-}$ considerably for some hydroxyl quinones, but this may as well be due to wider delocalization and not solely due to hydrogen bonding[73],[74]. In addition, documented pK_a values of QH$^{\bullet}$ and QH$_2$ vastly differ and thus show that protonation is likewise less effective in stabilizing the radical than the fully reduced form. Parenthetically, this trend of extremely dissimilar pK_a values holds for the superoxide and peroxide couple as well (4.8[75] and 11.6[76] for HO$_2^{\bullet}$ and H$_2$O$_2$, respectively). In short, aqueous environment is more effective in stabilizing the fully reduced quinone species than the semiquinone radical.

In CaCTAQ, hydrogen bonding as well as protonation to the quinone is partially blocked. As hydrogen bonding and protonation promote the stability of the fully reduced quinone more than that of the semiquinone, the net effect of Ca^{2+} in water will be to stabilize the semiquinone and destabilize the fully reduced quinone. Hence, by Ca^{2+} a negative shift in E_2 and an overall negative shift in E_{ave} result, although the quinone itself becomes electrophilic.

3.5.2. DFT calculations

In order to test the validity of our explanation, DFT calculation was performed on three redox states of CTAQ and MCTAQ (M = Ca, Sr, Ba, Mg). The fully reduced state, QH⁻, was singly protonated at O1 (Fig. 3−15) so that the overall charge would be the same as in Q˙⁻. Firstly, bond length change upon reduction was observed (Table 3−2). Taking reduction in bond length as increase in bond strength, CTAQ and MCTAQ showed different trends that agreed well with our explanation. Specifically, R_{O2-M} decreased far more in going from CTAQ˙⁻ to CTAQH⁻ than in going from CTAQ to CTAQ˙⁻, supporting our suggestion that hydrogen bonding and protonation are more effective on the fully reduced quinone than on the semiquinone

radical. Incidentally, the calculated length of semiquinone hydrogen bond agreed closely with the value obtained for the semiquinone radical anion of vitamin K_1 from EPR measurement (1.64 Å)[77]. MCTAQ all showed an opposite trend in R_{O2-M}, which is natural if the interaction between M^{2+} and the quinone is primarily ionic. In addition, R_{C4-O2} in the fully reduced quinone was also different for CTAQ and MCTAQ. Significant elongation in the former indicated that strong bond with proton caused the carbon−oxygen bond to weaken.
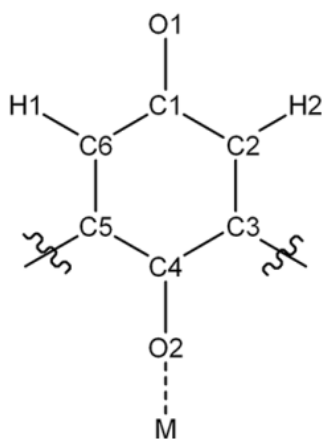

Fig. 3−15 Labeling scheme used for DFT calculation of the quinone moiety in CTAQ and MCTAQ. The lines do not indicate bond order. For CTAQ, M is a hydrogen atom from one of the carboxylic substituents that approached the quinone upon geometry optimization.

Secondly, reasoning that larger delocalization of electrons likely brings more stability[78], the sum of atomic mulliken charge densities on the quinone moiety, denoted as the quinone group charge density (Q), was obtained[79]. The change in Q upon reduction (ΔQ) was used as a measure of the degree of delocalization and stability. For instance, for the first reduction, ΔQ without any delocalization would be -1. Its relatively positive value for CaCTAQ implies there is a strong delocalization of the additional electron density over the entire molecule[80], which may account for the stabilizing effect of Ca^{2+} on Q•−. The ΔQ value was more positive for smaller metal ions having higher Lewis acidity, and it was the most negative for CTAQ. Upon second reduction to QH−, however, free CTAQ showed more positive ΔQ, indicating that the added electron is more delocalized in CTAQH− than in MCTAQH−. Considering the bond length results, this may be ascribed to bond formation between O2 and a proton from carboxylic acid. There was no perceptible trend in the value of ΔQ for second reduction among different metal ions, but it is evident that the metal ion is not as effective as proton in stabilizing the fully reduced quinone.

Table 3-2 Calculation results of the three redox states of CTAQ and MCTAQ.[a]

Parameters		CTAQ	MCTAQ			
			Ca^{2+}	Sr^{2+}	Ba^{2+}	Mg^{2+}
R_{C1-O1}	Q	1.22116	1.21989	1.22040	1.22059	1.21993
	Q•−	1.25415	1.25367	1.25418	1.25444	1.25274
	QH−	1.37385	1.38213	1.38269	1.38317	1.37997
R_{C4-O2}	Q	1.22198	1.22824	1.22853	1.22836	1.23075
	Q•−	1.28521	1.27991	1.2785	1.27753	1.28820
	QH−	1.34570	1.29704	1.29496	1.29420	1.30628
R_{O2-M}	Q	1.91245	2.33670	2.49719	2.66881	2.09816
	Q•−	1.61126	2.22434	2.38417	2.53352	1.91172
	QH−	1.00503	2.19272	2.34873	2.49712	1.88486
ΔQ^b	Q→Q•−	−0.412	−0.172	−0.287	−0.307	−0.062
	Q•−→QH−	0.321	−0.009	−0.123	−0.084	−0.032

[a]R is bond length in Å. Atom labels in the subscript follow Fig. 3-15.

[b]Q is the sum of Mulliken charges of atoms labeled with a number in Fig. 3-15 (six carbon, two oxygen, two hydrogen atoms in total).

Therefore, our argument regarding the different stabilities of quinone species was supported by computational results.

In essence, the fact that Ca^{2+} can stabilize $Q^{\bullet-}$ more than water but cannot Q^{2-}, which is well−stabilized by water, gives rise to the interesting properties of CaCTAQ. However, if the Lewis acidity of the metal ion is so large that it can stabilize both $Q^{\bullet-}$ and Q^{2-}more than water, E_2 will not be shifted negatively. In fact, the initial, transient voltammogram of ZnCTAQ, which slowly precipitated out of the solution, implied such a possibility. We plan to further investigate this issue by synthesizing thiol−CTAQ that can be immobilized on electrode surface to prevent precipitation. Incidentally, the intermediate Lewis acidity of Ca^{2+} may account for its various roles in nature, as implied by a recent study that suggested Ca^{2+} acts to modulate the redox potential in the oxygen evolving complex (OEC) moderately[81].

4. Conclusions

In summary, CTAQ was taken as a model compound to study the influence of redox-inactive Ca^{2+} ion on quinones in buffered aqueous solutions. Its voltammetric response and properties were significantly altered in the presence of Ca^{2+}; an unusual wave separation was seen at basic pH, observed for the first time for quinones in buffered aqueous solutions, and the semiquinone radical anion was extremely stabilized as shown through the large reduction in K_{disp} and spectroscopic observation. Digital simulation, which was straightforward owing to wave separation, yielded quantitative information to account for these results, namely the positive and negative shift of E_1 and E_2. It also foretold a catalytic current in the presence of less than one-equivalent of Ca^{2+} arising from CaCTAQ species reducing and oxidizing CTAQ homogeneously. Then the shifts of E_1 and E_2 were explained by taking into account the surrounding aqueous environment, which has much stronger stabilizing effect on the dianion than on the radical, contrary to metal ions. The analysis presented in this work is expected to contribute to a clearer understanding of how metal ions influence PCET reactions in aqueous solutions. Hopefully this

will lead to interesting new applications that depend on tuning redox and acid－base properties, as hinted by some of our observations.

5. References

[1] Chambers, J. Q. *The Chemistry of Quinonoid Compounds*, (Patai, S.), pp. 737–791. John Wiley & Sons, Ltd.

[2] Chambers, J. Q. *The Chemistry of Quinonoid Compounds*, (Patai, S. & Rappaport, Z.), pp. 719–757. Great Britain: John Wiley & Sons.

[3] Osyczka, A., Moser, C. C., & Dutton, P. L. *Trends Biochem. Sci.* **2005**, *30*, 176.

[4] Gunner, M. R., Madeo, J., & Zhu, Z. *J. Bioenerg. Biomembr.* **2008**, *40*, 509.

[5] Roginsky, V. A., Pisarenko, L. M., Bors, W., & Michel, C. *J. Chem. Soc. Perkin Trans. 2* **1999**, 871.

[6] Song, Y. & Buettner, G. R. *Free Radic. Biol. Med.* **2010**, *49*, 919.

[7] Eggins, B. R. & Chambers, J. Q. *J. Electrochem. Soc.* **1970**, *117*, 186.

[8] Bailey, S. I. & Ritchie, I. M. *Electrochimica Acta* **1985**, *30*, 3.

[9] N. Gupta & Linschitz, H. *J. Am. Chem. Soc.* **1997**, *119*, 6384.

[10] Quan, M., Sanchez, D., Wasylkiw, M. F., & Smith, D. K. *J. Am. Chem. Soc.* **2007**, *129*, 12847.

[11] Guin, P. S., Das, S., & Mandal, P. C. *Int. J. Electrochem.* **2011**, *2011*, 1.

[12] Cukier, R. I. & Nocera, D. G. *Annu. Rev. Phys. Chem.* **1998**, *49*, 337.

[13] Weinberg, D. R., Gagliardi, C. J., Hull, J. F., Murphy, C. F., Kent, C. A., Westlake, B. C., Paul, A., Ess, D. H., McCafferty, D. G., & Meyer, T. J. *Chem. Rev.* **2012**, *112*, 4016.

[14] Fukuzumi, S. *Roles of Metal Ions in Controlling Bioinspired Electron−Transfer Systems. Metal Ion−Coupled Electron Transfer*, pp. 49–153. John Wiley & Sons.

[15] Fukuzumi, S. *Org. Biomol. Chem.* **2003**, *1*, 609.

[16] Andreini, C., Bertini, I., Cavallaro, G., Holliday, G. L., & Thornton, J. M. *JBIC J. Biol. Inorg. Chem.* **2008**, *13*, 1205.

[17] Eaton, D. R. *Inorg. Chem.* **1964**, *3*, 1268.

[18] Itoh, S. & Fukuzumi, S. *J. Mol. Catal. B Enzym.* **2000**, *8*, 85.

[19] Yuasa, J., Suenobu, T., & Fukuzumi, S. *ChemPhysChem* **2006**, *7*, 942.

[20] Itoh, S., Kawakami, H., & Fukuzumi, S. *J. Am. Chem. Soc.* **1998**, *120*, 7271.

[21] Wu, H., Zhang, D., Su, L., Ohkubo, K., Zhang, C., Yin, S., Mao, L., Shuai, Z., Fukuzumi, S., & Zhu, D. *J. Am. Chem. Soc.* **2007**, *129*, 6839.

[22] Fukuzumi, S., Okamoto, K., Yoshida, Y., Imahori, H., Araki, Y., & Ito, O. *J. Am. Chem. Soc.* **2003**, *125*, 1007.

[23] Kay, C. W. M., Mennenga, B., Görisch, H., & Bittl, R. *J. Am. Chem. Soc.* **2005**, *127*, 7974.

[24] Sato, A., Takagi, K., Kano, K., Kato, N., Duine, J., & Ikeda, T. *Biochem J* **2001**, *357*, 893.

[25] Bogeski, I., Gulaboski, R., Kappl, R., Mirceski, V., Stefova, M., Petreska, J., & Hoth, M. *J. Am. Chem. Soc.* **2011**, *133*, 9293.

[26] Lebedev, A. V., Ivanova, M. V., Timoshin, A. A., & Ruuge, E. K. *ChemPhysChem* **2007**, *8*, 1863.

[27] Lebedev, A. V., Ivanova, M. V., & Ruuge, E. K. *Arch. Biochem. Biophys.* **2003**, *413*, 191.

[28] Itoh, S., Kawakami, H., & Fukuzumi, S. *Chem. Commun.* **1997**, 29.

[29] Morita, Y., Agawa, T., Kai, Y., Kanehisa, N., Kasai, N., Nomura, E., & Taniguchi, H. *Chem. Lett.* **1989**, *18*, 1349.

[30] Gomez-Kaifer, M., Reddy, P. A., Gutsche, C. D., & Echegoyen, L. *J. Am. Chem. Soc.* **1994**, *116*, 3580.

[31] Chung, T. D. & Kim, H.-S. *J. Incl. Phenom. Mol. Recognit. Chem.* **1998**, *32*, 179.

[32] Taek-Dong Chung, Sun-Kil Kang, Ha-suck Kim, Kim, J. R., Oh, W. S., & Chang, S.-K. *Chem. Lett.* **1998**, 1225.

[33] Kang, S.-K., Chung, T.-D., & Kim, H. *Electrochimica Acta* **2000**, *45*, 2939.

[34] Gamage, R. S. K. A., McQuillan, A. J., & Peake, B. M. *J. Chem. Soc. Faraday Trans.* **1991**, *87*, 3653.

[35] Li, Q., Batchelor-McAuley, C., Lawrence, N. S., Hartshorne, R. S., & Compton, R. G. *Chem. Commun.* **2011**, *47*, 11426.

[36] Eugene A. Permyakov & Robert H. Kretsinger Calcium binding proteins Singapore: John Wiley & Sons.

[37] Yocum, C. F. *Coord. Chem. Rev.* **2008**, *252*, 296.

[38] Costentin, C., Robert, M., & Savéant, J.-M. *Chem. Rev.* **2010**, *110*, PR1.

[39] Zhao, Y. & Truhlar, D. G. *Theor. Chem. Acc.* **2008**, *120*, 215.

[40] Hay, P. J. & Wadt, W. R. *J. Chem. Phys.* **1985**, *82*, 270.

[41] Papajak, E. & Truhlar, D. G. *J. Chem. Theory Comput.* **2010**, *6*, 597.

[42] M. J. Frisch Gaussian 09, revision B.01 Wallingford, CT: Gaussian Inc.

[43] Park, H., Oyama, M., Shim, Y.-B., & Okazaki, S. *J. Electroanal. Chem.* **2000**, *484*, 131.

[44] Bard, A. J. & Faulkner, L. R. Electrochemical Methods: Fundamentals and Applications United States: Wiley.

[45] Kang, S.-K., Lee, O.-S., Chang, S.-K., Chung, D.-S., Kim, H.-S., & Chung, T.-D. *Bull. Korean Chem. Soc.* **2011**, *32*, 793.

[46] Roginsky, V. A., Pisarenko, L. M., Bors, W., Michel, C., & Saran, M. *J. Chem. Soc. Faraday Trans.* **1998**, *94*, 1835.

[47] Alegria, A. E., Lopez, M., & Guevara, N. *J. Chem. Soc. Faraday Trans.* **1996**, *92*, 4965.

[48] Kaim, W. & Fiedler, J. *Chem. Soc. Rev.* **2009**, *38*, 3373.

[49] Zhao, X., Imahori, H., Zhan, C.-G., Sakata, Y., Iwata, S., & Kitagawa, T. *J. Phys. Chem. A* **1997**, *101*, 622.

[50] Tang, Y., Wu, Y., & Wang, Z. *J. Electrochem. Soc.* **2001**, *148*, E133.

[51] Park, H., Won, M.-S., Cheong, C., & Shim, Y.-B. *Electroanalysis* **2002**, *14*, 1501.

[52] Anxolabéhère-Mallart, E., Costentin, C., Policar, C., Robert, M., Savéant, J.-M., & Teillout, A.-L. *Faraday Discuss.* **2010**, *148*, 83.

[53] Medina-Ramos, J., Oyesanya, O., & Alvarez, J. C. *J. Phys. Chem. C* **2013**, *117*, 902.

[54] Song, N., Gagliardi, C. J., Binstead, R. A., Zhang, M.-T., Thorp, H., & Meyer, T. J. *J. Am. Chem. Soc.* **2012**, *134*, 18538.

[55] Laviron, E. *J. Electroanal. Chem.* **1984**, *169*, 29.

[56] Bishop, C. A. & Tong, L. K. J. *J. Am. Chem. Soc.* **1965**, *87*, 501.

[57] Patel, K. B. & Willson, R. L. *J. Chem. Soc. Faraday Trans. 1 Phys. Chem. Condens. Phases* **1973**, *69*, 814.

[58] P. Wardman *J Phys Chem Ref Data* **1989**, *18*, 1637.

[59] Shoup, D. & Szabo, A. *J. Electroanal. Chem. Interfacial Electrochem.* **1982**, *140*, 237.

[60] Ji, X., Banks, C. E., Silvester, D. S., Wain, A. J., & Compton, R. G. *J. Phys. Chem. C* **2007**, *111*, 1496.

[61] Batchelor-McAuley, C., Li, Q., Dapin, S. M., & Compton, R. G. *J. Phys. Chem. B* **2010**, *114*, 4094.

[62] Batchelor-McAuley, C., Kozub, B. R., Menshykau, D., & Compton, R. G. *J. Phys. Chem. C* **2011**, *115*, 714.

[63] Compton, R. G. & Banks, C. E. Understanding Voltammetry Singapore: World Scientific Publishing.

[64] Laviron, E. *J. Electroanal. Chem. Interfacial Electrochem.* **1983**, *146*, 15.

[65] Laviron, E. *J Electroanal Chem Interfacial Electrochem* **1984**, *164*, 213.

[66] Laviron, E. *J. Electroanal. Chem.* **1986**, *208*, 357.

[67] Pedersen, J. A. *Spectrochim. Acta. A. Mol. Biomol. Spectrosc.* **2002**, *58*, 1257.

[68] Fukuzumi, S., Nakanishi, I., Maruta, J., Yorisue, T., Suenobu, T., Itoh, S., Arakawa, R., & Kadish, K. M. *J. Am. Chem. Soc.* **1998**, *120*, 6673.

[69] Zhang, L., Bandy, B., & Davison, A. J. *Free Radic. Biol. Med.* **1996**, *20*, 495.

[70] Stegmann, H. B., Bergler, H. U., & Scheffler, K. *Angew. Chem. Int. Ed. Engl.* **1981**, *20*, 389.

[71] Kawashima, T., Ohkubo, K., & Fukuzumi, S. *Phys. Chem. Chem. Phys.* **2011**, *13*, 3344.

[72] Evans, D. H. & Lehmann, M. W. *Acta Chem. Scand.* **1999**, *53*, 765.

[73] Aguilar-Martinez, M., Macías-Ruvalcaba, N. A., Bautista-Martínez, J. A., Gómez, M., González, F. J., & González, I. *Curr. Org. Chem.* **2004**, *8*, 1721.

[74] Ashnagar, A., Bruce, J. M., Dutton, P. L., & Prince, R. C. *Biochim. Biophys. Acta BBA-Gen. Subj.* **1984**, *801*, 351.

[75] Bielski, B. H. J., Cabelli,, D. E., Arudi, R. L., & Ross, A. B. *J Phys Chem Ref Data* **1985**, *14*, 1041.

[76] Dean, J. A. Lange's Handbook of Chemistry McGraw-Hill.

[77] Niklas, J., Epel, B., Antonkine, M. L., Sinnecker, S., Pandelia, M.-E., & Lubitz, W. *J. Phys. Chem. B* **2009**, *113*, 10367.

[78] Oh, J.-W., Lee, Y. O., Kim, T. H., Ko, K. C., Lee, J. Y., Kim, H., & Kim, J. S. *Angew. Chem. Int. Ed.* **2009**, *48*, 2522.

[79] Zhang, C. *J. Hazard. Mater.* **2009**, *161*, 21.

[80] Wheeler, D. E., Rodriguez, J. H., & McCusker, J. K. *J. Phys. Chem. A* **1999**, *103*, 4101.

[81] Tsui, E. Y., Tran, R., Yano, J., & Agapie, T. *Nat. Chem.* **2013**, *5*, 293.

Abstract in Korean (국문초록)

캘릭사렌−삼산−퀴논(Calix[4]arene−triacid−monoquinone, CTAQ)은 퀴논 작용기를 가지고 있고 수용성인 이오노포어(ionophore)이다. 우리는 이 분자를 가지고 산화환원 반응성이 없는 금속 이온이 퀴논의 수용액에서의 양성자 수반 전자 전달(PCET) 반응에 어떤 영향을 주는지 연구하였다. 이 퀴논 이오노포어는 칼슘 이온을 붙잡을 수 있었고, 붙잡힌 칼슘 이온은 퀴논의 전기화학 거동을 크게 바꾸어 놓았다. 칼슘−CTAQ 복합체의 pH 에 의존하는 전기화학 거동과 특이한 산화환원 전위 갈라짐을 통해 메커니즘을 분석할 수 있었다. 분광학과 전기화학을 결합함으로써 중간체 세미퀴논이 안정해진다는 것을 확인할 수 있었고, 칼슘−CTAQ 복합체가 칼슘 이온을 붙잡지 않은 CTAQ 를 산화환원 시킬 때 전자전달 매개체로 작용하는 것도 관찰하였다. 순환 전압 전류법(cyclic voltammetry)으로 얻은 데이터를 컴퓨터로 시뮬레이션하였고, 이를 통해 우리의 여러 가지 실험 결과들을 설명할 수 있는 간단한 메커니즘을 칼슘 이온에 의한 퀴논의 열역학적 성질 변화에 기초하여 제안하였다. 이는 칼슘 이온의 정전기적 영향과 분자를 둘러싸고 있는 물분자의 수소결합의 영향으로 이해할 수 있었고, 이 설명을 뒷받침하기 위해 DFT 계산을 수행하였다.